INTERNATIONAL JOURNAL FOR NUMERICAL METHODS IN FLUIDS, VOL. 10, 199–211 (1990)

A CONTROL VOLUME FINITE DIFFERENCE METHOD FOR BUOYANT FLOW IN THREE-DIMENSIONAL CURVILINEAR NON-ORTHOGONAL CO-ORDINATES

H. Q. YANG* AND K. T. YANG

Department of Aerospace and Mechanical Engineering, University of Notre Dame, Notre Dame, IN 46556, U.S.A.

AND

J. R. LLOYD

Department of Mechanical Engineering, Michigan State University, East Lansing, MI 48824, U.S.A.

SUMMARY

This paper presents a control-volume-based finite difference method in non-orthogonal curvilinear co-ordinates on a local basis in which the vectors and tensors are all based on the general curvilinear co-ordinates for buoyant flow calculations in arbitrary three-dimensional geometries. The governing equations are transformed from Cartesian co-ordinates into generalized curvilinear co-ordinates. After integrating the set of equations for the control volumes, the finite difference equations are then formulated by a proper treatment of the heat flux and stress tensors and by incorporating the QUICK scheme for the convective terms. The solution procedure then follows the one for three-dimensional Cartesian co-ordinates.

Examples are given in problems of natural convection in such three-dimensional enclosures as parallelepiped enclosures and horizontal closed cylinders with differentially heated ends. In the latter case, important applications have been found in crystal growth by means of chemical vapour deposition in a cylindrical ampoule, in which uniform heat fluxes along the two ends are required in order to produce high-quality crystals. Special attention is given to the insertion of baffles in the cylinder to improve the recirculating flow patterns near the two ends.

KEY WORDS Finite difference Natural convection Enclosure flow Non-orthogonal co-ordinates

1. INTRODUCTION

Computation of heat transfer and fluid flow in complex geometries has always been a challenge to numerical analysts. Among the many approaches proposed, the body-fitted co-ordinate technique seems to have attracted much attention. The advantages of this technique are that the computational domain can be divided into curvilinear and non-orthogonal meshes so that they coincide with the physical boundary, and the governing equations are transformed into simpler forms. There is, however, a resulting complexity in that the vectors and tensors in rectangular co-ordinates must be transformed to those in body-fitted coordinates accordingly. Thus in the calculation procedure the dependent variables remain in Cartesian co-ordinates while the

* Present address: CFD Research Corporation, Huntsville, AL 35805, U.S.A.

0271–2091/90/020199–13$06.50

Received 14 December 1987
Revised 16 January 1989

conservation governing equations are expressed in terms of curvilinear control volumes. The transformation is needed in all control volume calculations. The purpose of this paper is to present an alternative approach in which the dependent variables and conservation equations are all expressed in curvilinear coordinates, sometimes known as a local basis approach in that the vectors and tensors are all based on general curvilinear co-ordinates. The advantage of this technique is that the unknowns and the conserved quantities are already in curvilinear co-ordinates so that no transformation is required during the calculations, a fact which makes the calculations more efficient. In both methods, however, the transformation of the governing equations is needed, but the final forms are different. In the body-fitted co-ordinate approach the momentum equations are all taken to be scalar so that the mass, energy and momentum equations are all in scalar form. For the present method, which is on the local basis, the variation of the co-ordinate lines of the base vector with position has to be taken into account. This variation results in additional terms with the Christoffel symbol in the momentum equations, a fact which seems to give rise to difficulties in the numerical discretization and solution. As will be shown, however, once proper treatment is taken on the Christoffel symbol a routine procedure can be followed, and a modification of the computer code in Cartesian co-ordinates can be made so that the code can be just as readily applied to curvilinear co-ordinates.

The present local basis co-ordinate system can be equally applied to cylindrical and spherical-polar co-ordinates. In fact, Raithby *et al.*[1] have proposed a methodology in two-dimensional orthogonal co-ordinates which is on the local basis. As far as non-orthogonal co-ordinates are concerned, Faghri *et al.*[2] have developed a solution methodology for convection–diffusion problems in which one boundary of the solution domain does not lie along the rectangular co-ordinate lines. In their derivation one of the two co-ordinate lines is transformed to a curvilinear non-orthogonal co-ordinate line while the other is kept along the rectangular line. The transformation procedure is rather elaborate and the extension to two co-ordinate lines will be expected to be even more complicated. Chen and Somerville[3] applied a co-ordinate transformation to the calculation of the flow above an irregular lower boundary where two of the co-ordinates (θ^1, θ^2) are along the usual Cartesian co-ordinates (x^1, x^2) but the third (θ^3) is a function of (x^1, x^2). Yang *et al.*[4] transformed the conservation equations into those in curvilinear co-ordinates and then, by using special properties of the geometry, obtained a set of reasonably simple equations for the problem of parallelpiped geometry. The focus of this paper is on the general approach without any simplification due to the geometry. The governing equations are transformed into those in non-orthogonal co-ordinates by a tensor transformation which retains the relatively simple forms. With a proper treatment of the heat flux and shear stress terms the discretization can be made directly on a physical basis, so that the physical interpretation of the terms can be readily made.

2. MATHEMATICAL FORMULATIONS

2.1. Conservation equations in generalized curvilinear co-ordinates

The conservative equations of mass, momentum and energy in Cartesian co-ordinates read as follows:

$$\rho_t + (\rho u_i)_{,i} = 0, \tag{1}$$

$$(\rho u_i)_t + (\rho u_i u_j)_{,j} = -p_{,i} + \rho G_i + \sigma_{ij,j}, \tag{2}$$

$$(\rho c_{\mathrm{pm}} T)_t + (\rho c_{\mathrm{pm}} u_i T)_{,i} = (kT_{,i})_{,i} + \mu\Phi - p u_{i,i}. \tag{3}$$

All the symbols are defined in the Appendix. Here the shear stress tensor σ_{ij} is given by

$$\sigma_{ij} = \mu(u_{i,j} + u_{j,i} - \tfrac{2}{3}\delta_{ij}u_{k,k}), \tag{4}$$

the dissipation function by

$$\Phi = 2(u_{i,j}^2)\delta_{ij} + [u_{i,j}(1 - \delta_{ij})]^2 - \tfrac{2}{3}(u_{i,i})^2 \tag{5}$$

and the mean specific heat by

$$c_{pm} = \int_{T_R}^{T} c_p(T)\,\mathrm{d}T/(T - T_R). \tag{6}$$

To transform the above set of equations into those in generalized curvilinear co-ordinates $(\theta^1, \theta^2, \theta^3)$, two rules in accordance with Eringen[5] are followed: (a) the partial differentiation symbol (,) is replaced by the covariant differentiation symbol (;); (b) the repeat indices are on the diagonal positions. Meanwhile, the physical components $u^{(i)}$ and $\sigma^{(kj)}$ are introduced according to the relations

$$u^i = u^{(i)}/h_i, \qquad u_i = g_{ij}u^{(j)}/h_j, \qquad \sigma_i^j = g_{ik}\sigma^{(kj)}/(h_k/h_j). \tag{7}$$

Here g_{ij} is the covariant metric tensor while g^{ij} in the following is the contravariant metrix tensor; h_i is the scale factor for curvilinear co-ordinates in directions θ^i. It is not a component, therefore the summation rule does not apply to the index of h_i.

For simplification the parentheses are dropped from now on and all the components are meant to be the physical ones. Equations (1)–(5) can now be recast into

$$\rho_t + (\rho u^i/h_i)_{;i} = 0, \tag{8}$$

$$(\rho g_{ik}u^k/h_k)_t + [\rho g_{ik}u^k u^j/(h_k h_j)]_{;j} = -p_{;i} + \rho g_{ij}G^j/h_j + [g_{ik}\sigma^{kj}/(h_k h_j)]_{;j}, \tag{9}$$

$$(\rho c_{pm}T)_t + (\rho c_{pm}u^i/h_i T)_{;i} = (kT_{;j}g^{ji})_{;i} + \mu\Phi - p(u^i/h_i)_{;i}. \tag{10}$$

The shear stresses now become

$$\sigma^{kj} = \mu h_k h_j[(u^j/h_j)_{;m}g^{mk} + (u^k/h_k)_{;m}g^{mj} - \tfrac{2}{3}\delta^{kj}(u^m/h_m)_{;m}] \tag{11}$$

and the dissipation function becomes

$$\Phi = 2[(u^i/h_i)_{;j}]^2\delta_i^j + [(u^i/h_i)_{;j}(1 - \delta_i^j)]^2 - \tfrac{2}{3}[(u^i/h_i)_{;i}]^2. \tag{12}$$

In the above equations the covariant differentiation is the partial derivative of a scalar (say p), a vector (say u^i) or a tensor (say σ^{ij}) with respect to the curvilinear system θ^i. For a scalar

$$p_{;i} = p_{,i}, \tag{13}$$

for a vector

$$u^i_{;i} = u^i_{,i} + \begin{Bmatrix} i \\ im \end{Bmatrix} u^m = g^{-1/2}(g^{1/2}u^i)_{,i} \tag{14}$$

and for a tensor

$$\sigma^{ij}_{;j} = \sigma^{ij}_{,j} + \begin{Bmatrix} i \\ jm \end{Bmatrix}\sigma^{mj} + \begin{Bmatrix} j \\ jm \end{Bmatrix}\sigma^{im} = g^{-1/2}(g^{1/2}\sigma^{ij})_{,j} + \begin{Bmatrix} i \\ jm \end{Bmatrix}\sigma^{mj}, \tag{15}$$

where g is the determinant of the covariant metric tensor,

$$g = |g_{ij}|. \tag{16}$$

$\{{}^{i}_{jm}\}$ is known as the Christoffel symbol of the second kind and is given by

$$\left\{ \begin{matrix} i \\ jm \end{matrix} \right\} = \frac{\partial x^k}{\partial \theta^j \partial \theta^m} \frac{\partial \theta^i}{\partial x^k} = (g^{ik}/2)[(g_{jk})_{,m} + (g_{mk})_{,j} - (g_{jm})_{,k}]. \tag{17}$$

The following properties of g have been utilized above:

$$(\log g^{1/2})_{,j} = \left\{ \begin{matrix} m \\ mj \end{matrix} \right\} \tag{18}$$

and the metric tensors satisfy

$$g_{ik} g^{kj} = \delta^j_i, \tag{19}$$

$$(g_{ik})_{;j} = 0. \tag{20}$$

Equation (19) has been used to find the contravariant metric tensor. By realizing the tensorial property of the term $u^i u^j$, a momentum flux is defined as follows:

$$M^{ij} = \rho u^i u^j - \sigma^{ij}. \tag{21}$$

With (14), (15), (20) and (21), equations (8)–(10) can now be written as

$$\rho_t + g^{-1/2}(g^{1/2} \rho u^i / h_i)_{,i} = 0, \tag{22}$$

$$(\rho u^i / h_i)_t + g^{-1/2}[g^{1/2} M^{ij}/(h_i h_j)]_{,j} + \left\{ \begin{matrix} i \\ jm \end{matrix} \right\} M^{jm}/(h_j h_m) = -p_{,k} g^{ki} + \rho G^i / h_i, \tag{23}$$

$$(\rho c_{\mathrm{pm}} T)_t + g^{-1/2}(g^{1/2} \rho u^i / h_i c_{\mathrm{pm}} T)_{,i} = g^{-1/2}(g^{1/2} k T_{,j} g^{ji})_{,i} + \mu \Phi - p g^{-1/2}(g^{1/2} u_i)_{,i}. \tag{24}$$

Some manipulations are required so that the momentum equation can have a form similar to (24). First, recalling the definition of M^{ij} along with σ^{ij} in (11) and that of $\{{}^{i}_{jm}\}$ in (17), it is found that j and m are exchangeable, so that

$$\left\{ \begin{matrix} i \\ jm \end{matrix} \right\} M^{jm}/(h_j h_m) = (g^{ik}/2)[2(g_{jk})_{,m} - (g_{jm})_{,k}] M^{jm}/(h_j h_m). \tag{25}$$

Secondly, h_i is removed from the denominator. Equation (23) now becomes

$$\begin{aligned}(\rho u^i)_t + g^{-1/2}[g^{1/2} M^{ij}/(h_j)]_{,j} = {} & -p_{,j} g^{ji} h_i + \rho G^i + (h_i)_{,j} M^{ij}/(h_i h_j) \\ & - (g^{ik}/2)[2(g_{jk})_{,m} - (g_{jm})_{,k}] M^{jm} h_i/(h_j h_m).\end{aligned} \tag{26}$$

2.2. Control volume finite difference equations

To solve the above sets of equations by the control volume finite difference method, a grid is first generated to cover the whole domain of interest. Figure 1 shows a typical two-dimensional curvilinear control volume system which is bounded by the physical boundary and is non-orthogonal. A staggered grid system has been adopted, i.e. the scalar variables (p, ρ, T, etc.) are located at the centre of the base control volume, while the velocity components u^1, u^2 and u^3 are located at the surfaces of the base control volume which are shifted half a cell towards the west, north and out of the paper respectively. In the control volume method the equations are discretized by integrating the conservation equations over the curvilinear control volume, which is bounded by lines of constant θ^1, θ^2 and θ^3. In non-orthogonal co-ordinates the differential area is given by the cross-product of two vectors which bound it, i.e.

$$\Delta \mathbf{A} = \Delta \theta^i \mathbf{g}_i \times \Delta \theta^j \mathbf{g}_j = g^{1/2} e_{ijk} \Delta \theta^i \Delta \theta^j / h_k \mathbf{g}^k, \tag{27}$$

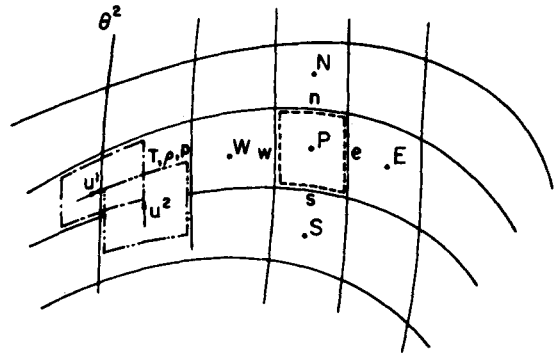

Figure 1. Control volumes and nodal points

and the differential volume is given by

$$\Delta v = \Delta \mathbf{A} \cdot \Delta\theta^m \mathbf{g}_m = g^{1/2} e_{ijk} \Delta\theta^i \Delta\theta^j \Delta\theta^k, \tag{28}$$

where e_{ijk} is the permutation symbol:

$$e_{ijk} = \begin{cases} 1 & \text{if } i, j, k \text{ are cyclic,} \\ -1 & \text{if } i, j, k \text{ are anticyclic,} \\ 0 & \text{if } i, j, k \text{ are acyclic.} \end{cases}$$

With the above relations, the conservation equation of mass after integrating over the control volume around P can be written as

$$(\rho)_t \Delta v + G_e^1 A_e - G_w^1 A_w + G_n^2 A_n - G_s^2 A_s + G_f^3 A_f - G_b^3 A_b = 0. \tag{29}$$

Here G^i is the mass flow rate in the direction θ^i, i.e.

$$G^i = \rho u^i, \tag{30}$$

and the area A and the volume are all in the physical space:

$$\begin{aligned} A_{e,w} &= g^{1/2}/h_1 \Delta\theta^2 \Delta\theta^3|_{e,w}, \\ A_{n,s} &= g^{1/2}/h_2 \Delta\theta^3 \Delta\theta^1|_{n,s}, \\ A_{f,b} &= g^{1/2}/h_3 \Delta\theta^1 \Delta\theta^2|_{f,b}. \end{aligned} \tag{31}$$

Integration of the energy equation results in

$$(\rho c_{pm} T)_t \Delta v + J_e^1 A_e - J_w^1 A_w + J_n^2 A_n - J_s^2 A_s + J_f^3 A_f - J_b^3 A_b = S^T. \tag{32}$$

Here J^i is the total heat flux including conduction and convection along the direction θ^i, i.e.

$$J^i = G^i c_{pm} T - (k T_{,j} g^{ij} h_i), \tag{33}$$

and S^T is the heat source term including viscous dissipation as well as pressure work:

$$S^T = (\mu\Phi + p g^{-1/2} (g^{1/2} u^i)_{,i}) \Delta v. \tag{34}$$

For the momentum equation we then have

$$(\rho u^i)_t \Delta v + M_e^{i1} A_e - M_w^{i1} A_w + M_n^{i2} A_n - M_s^{i2} A_s + M_f^{i3} A_f - M_b^{i3} A_b = (-p_{,j} g^{ij} h_i + \rho G_i) \Delta v + S^i, \tag{35}$$

where S^i includes the force due to curvilinear non-orthogonality of the co-ordinates:

$$S^i = [(h_i)_{,j} M^{ij}/(h_i h_j)]\Delta v - \Delta v[g^{ik}/2(2(g_{jk})_{,m} - (g_{jm})_{,k})M^{jm}h_i/(h_j h_m)]. \tag{36}$$

The next step is to approximate all the flux terms (J^i, M^{ij}) and source terms (S^T, S^i). Owing to the non-orthogonality, the simple Fourier form of conducting heat flux, for example, is in a derivative form involving multidirections, as are the stress terms (equation (11)). A stress–flux formulation due to Raithby *et al.*[1] in two-dimensional orthogonal co-ordinates is incorporated here so that

$$J^i = G^i c_{\mathrm{pm}} T - kT_{,i} g^{ii} h_i + (kT_{,i} g^{ii} h_i - k_{,j} g^{ij} h_i) = \hat{J}^i + (kT_{,i} g^{ii} h_i - kT_{,j} g^{ij} h_i), \tag{37}$$

$$M^{ij} = G^j u^i - \mu u^i_{,j} g^{jj} h_j + (\mu u^i_{,j} g^{jj} h_j - \sigma^{ij}) = \hat{M}^{ij} + (\mu u^i_{,j} g^{jj} h_j - \sigma^{ij}), \tag{38}$$

and for the pressure gradient

$$-p_{,j} g^{ij} h_i = -p_{,i} g^{ii} h_i + (p_{,i} g^{ii} h_i - p_{,j} g^{ij} h_i). \tag{39}$$

By using the average pressure, the source term of (34) can be written as

$$S^T = (\mu\Phi)\Delta v + p_{\mathrm{P}}(u^1_{\mathrm{e}} A_{\mathrm{e}} - u^1_{\mathrm{w}} A_{\mathrm{w}} + u^2_{\mathrm{n}} A_{\mathrm{n}} - u^2_{\mathrm{s}} A_{\mathrm{s}} + u^3_{\mathrm{f}} A_{\mathrm{f}} - u^3_{\mathrm{b}} A_{\mathrm{b}}). \tag{40}$$

Similarly, again using the average values, we can write (36) as

$$S^i = \sum_j \overline{(M^{ij}/h_i)_{\mathrm{P}}}(h_i A_j)|^{\mathrm{e,n,f}}_{\mathrm{w,s,b}} - \sum_{j,k,m} \overline{(g^{ik} M^{jm} h_i/h_j)_{\mathrm{P}}}(g_{jk} A_m)|^{\mathrm{e,n,f}}_{\mathrm{w,s,b}}$$
$$+ \sum_{j,k,m} \overline{[(g^{ik}/2)M^{jm} h_i h_k/(h_j h_m)]_{\mathrm{P}}}(g_{jm} A_k)|^{\mathrm{e,n,f}}_{\mathrm{w,s,b}}. \tag{41}$$

Now the energy and momentum equations become

$$(\rho c_{\mathrm{pm}} T)_t \Delta v + \hat{J}^1_{\mathrm{e}} A_{\mathrm{e}} - \hat{J}^1_{\mathrm{w}} A_{\mathrm{w}} + \hat{J}^2_{\mathrm{n}} A_{\mathrm{n}} - \hat{J}^2_{\mathrm{s}} A_{\mathrm{s}} + \hat{J}^3_{\mathrm{f}} A_{\mathrm{f}} - \hat{J}^3_{\mathrm{b}} A_{\mathrm{b}} = \hat{S}^T, \tag{42}$$

$$(\rho u^i)_t \Delta v + \hat{M}^{i1}_{\mathrm{e}} A_{\mathrm{e}} - \hat{M}^{i1}_{\mathrm{w}} A_{\mathrm{w}} + \hat{M}^{i2}_{\mathrm{n}} A_{\mathrm{n}} - \hat{M}^{i2}_{\mathrm{s}} A_{\mathrm{s}} + \hat{M}^{i3}_{\mathrm{f}} A_{\mathrm{f}} - \hat{M}^{i3}_{\mathrm{b}} A_{\mathrm{b}} = (-p_{,i} g^{ii} h_i + \rho G^i)\Delta v + \hat{S}^i, \tag{43}$$

where

$$\hat{S}^T = S^T - (kT_{,1} g^{11} h_1 - kT_{,j} g^{1j} h_1) A|^{\mathrm{e}}_{\mathrm{w}} - (kT_{,2} g^{22} h_2 - kT_{,j} g^{2j} h_2) A|^{\mathrm{n}}_{\mathrm{s}}$$
$$- (kT_{,3} g^{33} h_3 - kT_{,j} g^{3j} h_3) A|^{\mathrm{f}}_{\mathrm{b}}, \tag{44}$$

$$\hat{S}^i = S^i - (\mu u^i_{,1} g^{11} h_1 - \sigma^{i1}) A|^{\mathrm{e}}_{\mathrm{w}} - (\mu u^i_{,2} g^{22} h_2 - \sigma^{i2}) A|^{\mathrm{n}}_{\mathrm{s}} - (\mu u^i_{,3} g^{33} h_3 - \sigma^{i3}) A|^{\mathrm{f}}_{\mathrm{b}}$$
$$+ (p_{,i} g^{ii} h_i - p_{,j} g^{ij} h_i)\Delta v. \tag{45}$$

Care is to be taken in treating the flux terms. For example, in the heat flux terms J^i the term $c_{\mathrm{pm}} T$ is to be evaluated at the surfaces of the control volumes. To accomplish this, a QUICK scheme[6] is incorporated here:

$$\hat{J}^1_{\mathrm{w}} = (G^1 c_{\mathrm{pm}} T)_{\mathrm{w}} - (kT_{,1} g^{11} h_1)_{\mathrm{w}}$$
$$= G^1_{\mathrm{W}}(c_{\mathrm{pmW}} T_{\mathrm{W}} + c_{\mathrm{pmP}} T_{\mathrm{P}}) - (1/8)\mathrm{CURVN} + (1/24)\mathrm{CURVT1}$$
$$+ (1/24)\mathrm{CURVT2} - (kg^{11} h_1)_{\mathrm{w}}/\Delta\theta^1 (T_{\mathrm{P}} - T_{\mathrm{W}}). \tag{46}$$

Here CURVN is the stabilizing curvature term in the normal direction (θ^1-direction) and CURVT1 and CURVT2 are the stabilizing curvature terms in the transverse directions (θ^2- and θ^3-directions).[6] To satisfy the mass conservation equation, the pressure correction equation due to Patankar[7] can be applied. It is to be noted that the corrected velocity u^1 is related to the

approximated velocity u^{1*} as

$$u^1 = u^{1*} + (A/a g^{11} h_1 h_1)_w (p_p - p_w), \tag{47}$$

which shows that the coefficients in the pressure correction equation are to be multiplied by $g^{ii}h_i h_i$ compared to those for Cartesian co-ordinates.

The final general finite difference equation for the temperature variable can now be written as

$$a_P T_P = a_W T_W + a_E T_E + a_S T_S + a_N T_N + a_B T_B + a_F T_F + S. \tag{48}$$

Besides the source term S^T, S here also includes terms for all the neighbouring points of P (such as $A_{NW}T_{NW}$, $A_{SW}T_{SW}$, etc.). This practice will not result in any major increase in the number of coefficient updates since the equations are still in the iterative form. In fact, the properties such as σ^{ij}, conductive flux $kT_{,j}g^{ij}$ and terms due to the QUICK scheme ($A_{NW}T_{NW}$, $A_{SW}T_{SW}$, etc.) are evaluated from the last iteration. To obtain accurate non-linear solutions to within specified tolerances, several iterations are usually required.

3. RESULTS AND DISCUSSION

As demonstrated above, the solution procedure for a set of equations in non-orthogonal co-ordinates is very similar to the one in Cartesian co-ordinates. Proper modification can be made: (1) by introducing a stress tensor subroutine and a heat flux subroutine; (2) by adding source terms; and (3) by multiplying the coefficients in the pressure correction equation by $g^{ii}h_i h_i$. The key to discretization and transformation is the metric tensors g^{ij} and g_{ij}. These can be found algebraically or numerically. Since

$$g_{ij} = \mathbf{g}_i \cdot \mathbf{g}_j \tag{49}$$

and

$$g^{ij} = \mathrm{cof}(g_{ij})/|g|, \tag{50}$$

it is important to have the basic vector $\mathbf{g}_i$ in non-orthogonal co-ordinates first. This can be defined as

$$\mathbf{g}_i = \frac{\partial}{\partial \theta^i}(x^j \mathbf{e}_j) = \frac{\partial x^j}{\partial \theta^i}\mathbf{e}_j, \tag{51}$$

so that

$$g_{ij} = \mathbf{g}_i \cdot \mathbf{g}_j = \frac{\partial x^m}{\partial \theta^i}\frac{\partial x^m}{\partial \theta^j} \tag{52}$$

and

$$h_i = (\mathbf{g}_i \cdot \mathbf{g}_j)^{1/2} = \left(\frac{\partial x^m}{\partial \theta^i}\frac{\partial x^m}{\partial \theta^j}\right)^{1/2}. \tag{53}$$

Once the interrelation between x^i and θ^i is given, an algebraic expression can be derived directly. Another way to find the metric tensors is by numerical grid generation.[8]

In the following, two examples are used to demonstrate the application of the present methodology.

3.1. Buoyant flow in complex parallelepiped enclosures

The enclosure itself is shown in Figure 2. It is formed by skewing a rectangular enclosure along the z-axis by an angle γ and along the x-axis by an angle ψ. The length L, width W and height H

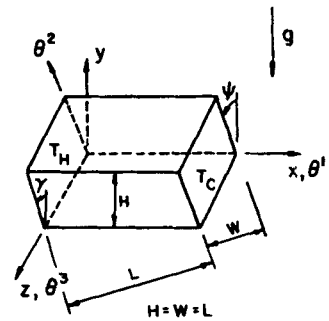

Figure 2. Parallelepiped enclosure geometry

are all perpendicular distances between the surfaces as shown in Figure 2. Through the geometrical relation we have

$$
\begin{aligned}
g^{11} &= 1/\cos^2\gamma, \\
g^{22} &= 1/\cos^2\gamma\cos^2\psi, \\
g^{33} &= (1-\sin^2\gamma\cos^2\psi)/(\cos^2\gamma\cos^2\psi), \\
g^{12} &= g^{21} = -\sin\gamma/(\cos^2\gamma\cos^2\psi), \\
g^{13} &= g^{31} = \sin\gamma\sin\psi/(\cos^2\gamma\cos\psi), \\
g^{23} &= g^{32} = -\sin\psi/(\cos^2\gamma\cos^2\psi).
\end{aligned}
\tag{54}
$$

Since the g^{ij} are independent of θ^i, the terms in (36) vanish, while all the other expressions remain. The calculation can be carried out for various combinations of angles γ and ψ.

The boundary conditions are also shown in Figure 2. Two parallel differentially heated walls incline from the vertical position at an angle γ, which is fixed at 30° in the present case. The top and bottom surfaces are horizontal and adiabatic, while the front and back walls incline at an angle ψ, which is varied from 0° to 45° to determine the three-dimensional effects. When ψ is 0° the motion is two-dimensional, except near the lateral wall regions owing to the viscous drag, as seen in Figure 3. As ψ increases, the flow in the θ^1–θ^2 plane becomes rather weak as can be seen by the value of the maximum streamfunction, and three-dimensionality becomes increasingly more significant as seen from the flow pattern in the θ^2–θ^3 plane. This three-dimensional motion is partially due to the insulated boundary at the inclined lateral walls, near which non-parallel and non-horizontal isotherms appear. At $\psi = 45°$ the motion in the θ^1–θ^2 plane is so slow that a dual cell appears.

The validation of the code with the above geometry with $\gamma = 0$ can be found in Reference 4 and hence will not be repeated here. The comparison of the numerical results with experimental data is considered to be very good.

3.2. Buoyant flow in a horizontal cylinder with internal baffles

The second example illustrated here is the natural convection inside a horizontal cylinder with differentially heated ends. One of the important applications of this problem is crystal growth in a closed ampoule. In general, it is required to have both high and uniform heat transfer rates at the end walls. However, these two requirements are contrary to each other in that a high heat transfer rate generated by natural convection is non-uniform in nature, while a uniform heat transfer rate

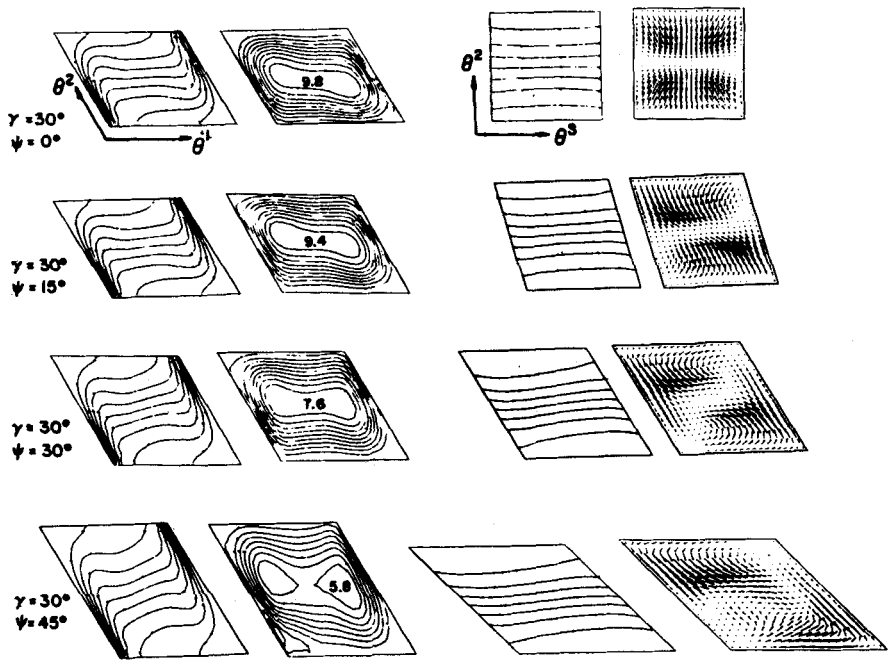

Figure 3. Temperature and velocity fields at $Ra = 10^5$, $Pr = 0{\cdot}71$ with various inclination angles

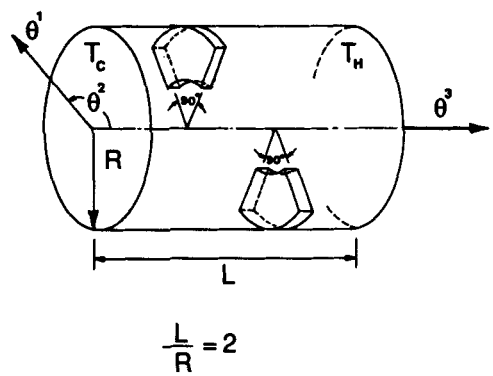

Figure 4. Horizontal cylinder with internal baffles

can be obtained only with pure conduction, which represents the lowest heat transfer rate. The compromise is to have a relatively high heat transfer rate with appropriate uniformity. This goal can be reached by proper control of natural convection. Many approaches have been proposed, e.g. inclining the cylinder with respect to gravity,[9] using both vertical and horizontal temperature gradients[9] and rotating the cylinder along the horizontal axis,[10] but the attention here is focused on the improvement of the uniformity of the heat flux at the two ends by inserting transverse azimuthal conducting baffles as shown in Figure 4. A set of orthogonal co-ordinates can be

applied to this geometry with the properties

$$g_{ij} = \delta_{ij} h_i h_j, \tag{55}$$

$$g^{ij} = \delta_{ij}/h_i h_j. \tag{56}$$

These equations make the treatment of the first derivative terms in the governing equation easier. For example, equation (37) now becomes

$$J^i = G^i c_{pm} T - kT_{,j} g^{ij} h_i = G^i c_{pm} T - kT_{,i} g^{ii} h_i = \hat{J}^i, \tag{57}$$

equation (39) becomes

$$-p_{,j} g^{ij} = -p_{,i} g^{ii} \tag{58}$$

and equation (41) can also be appropriately simplified as

$$S^i = \sum (M^{ij}/h_i)_P (h_i A_j)|_{w,s,b}^{e,n,f} - \sum (M^{im}/h_i^2)_P (h_i^2 A_m)|_{w,s,b}^{e,n,f} + \sum (M^{jj}/(2h_j^2))_P (h_j^2 A_i)|_{w,s,b}^{e,n,f}. \tag{59}$$

The results for a horizontal cylinder without internal baffle at various Rayleigh numbers have been validated and reported in Reference 11. Presently the calculation is carried out for a solid baffle with thermal conductivity ratio of solid to fluid (air) of 500. Comparison between the two cases is displayed in Figures 5 and 6.

Shown in Figure 5(a) are the isotherms and flow patterns in the vertical centreplane.[11] Owing to the circulation which is induced by the buoyancy force, the cold (hot) fluid directly impinges on the hot (cold) surface at the lower right (upper left) corner region. This leads to a relatively dense isotherm distribution corresponding to a high heat transfer rate. As the fluid ascends (descends) along the hot (cold) surface it becomes hotter (colder) so that the heat transfer rate decreases. At

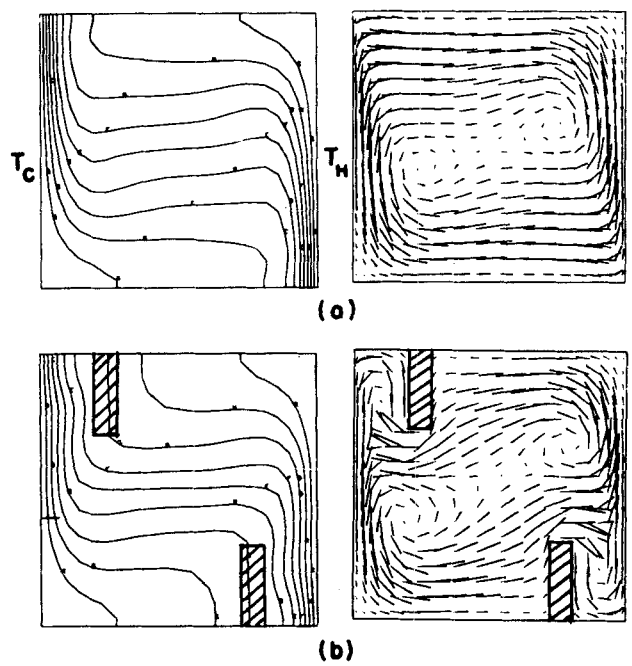

Figure 5. Temperature and velocity fields in the vertical central plane of a cylinder at $Ra = 10^5$, $Pr = 0{\cdot}71$ with and without baffles

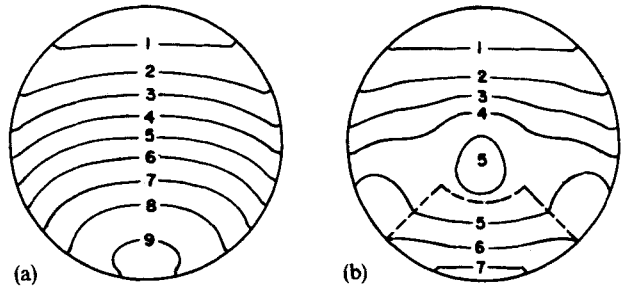

Figure 6. Nusselt number contour on the hot wall

the lower left (upper right) corner there results a minimum heat transfer rate. When two baffles are inserted into the enclosure as shown in Figure 4 they prevent the direct impingement so that the isotherms change their shape and give rise to a lower heat transfer rate as shown in Figure 5(b). This effect has also been clearly demonstrated in Figure 6, in which the local heat fluxes are represented by the Nusselt number contour on the hot surface. Figure 6(a) represents the case without baffles. It is seen that at the bottom part of the hot end surface a relatively high Nusselt number appears, and the gradient of the Nusselt number along the vertical direction is also very strong. The introduction of a high-conductivity baffle in the transverse flow direction counteracts the effect of the direct impingement so that the heat flux is reduced and the distribution becomes much more uniform as shown in Figure 6(b).

4. CONCLUSIONS

The governing equations in non-orthogonal curvilinear co-ordinates with contravariant velocity components as dependent variables in the momentum equations are derived through a tensor transformation. The finite difference equations based on control volumes are presented.

The advantages of using the contravariant component are its direct physical representation along the co-ordinate lines and the unnecessariness in the transformation between various components (such as transformation between Cartesian, covariant, contravariant projection and contravariant components). The trade-off here is a higher complexity in the equations. It is demonstrated that once proper treatment is made of the Christoffel symbol, a routine procedure can be followed and a straightforward modification of the computer algorithm in Cartesian co-ordinates can be made so that it can be just as readily applied to curvilinear co-ordinates.

Two simple examples have been used to demonstrate the present method. Further computations with more complicated scale factors and metric tensors will be carried out and reported later.

ACKNOWLEDGEMENT

The authors wish to acknowledge the support of the National Science Foundation under Grant CBT82-19158 to the University of Notre Dame and the University of Notre Dame Computer Center.

APPENDIX: NOMENCLATURE

A	area
a	coefficient in difference equations

c_p	isobaric specific heat
c_{pm}	mean specific heat
$\mathbf{e}_i$	basic vector in Cartesian co-ordinates, $i=1, 2, 3$
e_{ijk}	permutation symbol
g	determinant of covariant matrix tensor g_{ij}
$\mathbf{g}_i$	basic vector in curvilinear co-ordinates, $i=1, 2, 3$
g^{ij}, g_{ij}	contravariant, covariant metric tensors
G_i	gravitational acceleration vector, $i=1, 2, 3$
h_i	scale factor in θ^i-direction
H	height of enclosure
J^i	total heat flux in θ^i-direction
k	thermal conductivity
L	length of enclosure
M^{ij}	momentum flux in j-direction for velocity component u^i
Nu	Nusselt number, hL/k
P	static pressure
Pr	Prandtl number
r	radius co-ordinate
R	radius of cylinder
Ra	Rayleigh number, $\rho_R g\beta(T_H-T_C)L^3/\mu_R\alpha_R$
S	source term
T	temperature
u^i	velocity components $i=1, 2, 3$
v	control volume
W	width of enclosure
x^i	Cartesian co-ordinates, $i=1, 2, 3$
z	axial co-ordinate

Greek symbols

α	thermal diffusivity
β	volume expansion coefficient
γ	skewed angle along z-axis
ψ	skewed angle along x-axis
$\Delta\theta^i$	incremental independent variables, $i=1, 2, 3$
δ_{ij}	Kronecker delta
μ	dynamic viscosity
ρ	density
σ_{ij}	shear stress tensor
θ^i	orthogonal co-ordinates, $i=1, 2, 3$
Φ	dissipation function
Σ	summation symbol

Superscripts

$(\bar{\ })$	average value
T	with respect to energy equation
i	with respect to momentum equation in θ^i-direction

Subscripts

C	cold wall
H	hot wall
i, j, k	co-ordinate indices
t	time derivative
n, s, e, w, f, b	surface nodal designation of control volume
P, N, S, E, W, F, B	nodal designation of control volume
R	reference condition
(,)	spatial derivative

REFERENCES

1. G. D. Raithby, P. F. Galpin and J. P. Van Doormaal, 'Prediction of heat and fluid flow in complex geometries using general orthogonal coordinates', *Numer. Heat Transfer*, **9**, 125–142 (1986).
2. M. Faghri, E. M. Sparrow and A. T. Prata, 'Finite-difference solutions of convection–diffusion problems in irregular domains, using a nonorthogonal coordinate transformation', *Numer. Heat Transfer*, **7**, 183–209 (1984).
3. G. Chen and R. C. J. Somerville, 'On the use of a coordinate transformation for the solution of the Navier–Stokes equations', *J. Comput. Phys.*, **17**, 209–228 (1975).
4. H. Q. Yang, K. T. Yang and J. R. Lloyd, 'Buoyant flow calculations with non-orthogonal curvilinear coordinates for vertical and horizontal parallelepiped enclosures', *Int. j. numer. methods eng.*, **25**, 331–345 (1988).
5. A. C. Eringen, *Mechanics of Continua*, Wiley, New York, 1967.
6. H. Q. Yang, K. T. Yang and J. R. Lloyd, 'Laminar natural convection flow transition in tilted three-dimensional longitudinal rectangular enclosures', *Int. J. Heat Mass Transfer*, **30**, 1637–1644 (1987).
7. S. V. Patankar, *Numerical Heat Transfer and Fluid Flow*, Hemisphere, Washington DC, 1980.
8. J. F. Thompson (ed.), *Numerical Grid Generation*, North-Holland, Amsterdam, 1982.
9. A. Solan and S. Ostrach, 'Convection effects in crystal growth by closed-tube chemical vapor transport', in W. R. Wilcox (ed.), *Preparation and Properties of Solid State Materials, Vol. 4*, Marcel Dekker, New York, 1976, pp. 63–110.
10. H. Q. Yang, K. T. Yang and J. R. Lloyd, 'Rotational effects on natural convection in a horizontal cylinder', *AIChE J.* **34**, 1627–1633 (1988).
11. H. Q. Yang, K. T. Yang and J. R. Lloyd, 'Three-dimensional laminar buoyant flow in a horizontal cylinder with differentially-heated end walls at high Rayleigh numbers', *Numer. Heat Transfer*, **14**, 429–446 (1988).